OPEN

Light: Science & Applications (2016) 5, e16124; doi:10.1038/lsa.2016.124

www.nature.com/lsa

ORIGINAL ARTICLE

New function of the Yb^{3+} ion as an efficient emitter of persistent luminescence in the short-wave infrared

Yan-Jie Liang[1,2,*], Feng Liu[1,3,*], Ya-Fei Chen[1,2], Xiao-Jun Wang[4], Kang-Ning Sun[2] and Zhengwei Pan[1,3]

The trivalent ytterbium (Yb^{3+}) ion has been extensively used as an emitter in short-wave infrared (SWIR) lasers, a sensitizer to activate other lanthanide ions for up-conversion luminescence, and a spectral converter in Ln^{3+}-Yb^{3+} doubly doped quantum cutting phosphors. Here we report a new function of the Yb^{3+} ion—as an efficient emitting center for SWIR persistent luminescence. We have developed the first real SWIR persistent phosphor, $MgGeO_3$:Yb^{3+}, which exhibits very-long persistent luminescence at around 1000 nm for longer than 100 h. The $MgGeO_3$:Yb^{3+} phosphor is spectrally transparent to visible/near-infrared light (~400–900 nm) and is a promising ultraviolet-to-SWIR spectral convertor. The $MgGeO_3$:Yb^{3+} phosphor also exhibits a photostimulated persistent luminescence capability, where the SWIR persistent emission in an ultraviolet-light pre-irradiated sample can be rejuvenated by low-energy light (white or red light) stimulation. The $MgGeO_3$:Yb^{3+} phosphor is expected to have promising applications in biomedical imaging, night-vision surveillance and photovoltaics.
Light: Science & Applications (2016) **5,** e16124; doi:10.1038/lsa.2016.124; published online 29 July 2016

Keywords: persistent luminescence; photostimulation; short-wave infrared (SWIR); ytterbium ions (Yb^{3+})

INTRODUCTION

Persistent luminescence, also called afterglow, is a special optical phenomenon in which a material continues emitting for an appreciable time, from minutes to hours, after the stoppage of excitation[1,2]. Persistent phosphors emitting in the visible spectral region have been extensively studied, and some visible persistent phosphors, such as green-emitting $SrAl_2O_4$:Eu^{2+},Dy^{3+} (ref. 3) and blue-emitting $Sr_2MgSi_2O_7$:Eu^{2+},Dy^{3+} (ref. 4), have achieved commercial success and are widely used as night-vision materials in a variety of areas. In recent years, persistent luminescence in wavelengths beyond the visible spectral region, that is, in the near-infrared (NIR; ~700–900 nm) and the short-wave infrared (SWIR; 900–1700 nm) spectral regions, has received considerable attention because longer-wavelength persistent luminescence has many promising advanced applications, ranging from infrared night-vision surveillance to biomedical imaging. For example, for infrared night-vision surveillance, NIR light and SWIR light are invisible to the naked eye (need to be detected by NIR or SWIR detection devices), and SWIR light has high penetrating power in haze, fog, smoke and dust[5]. For biomedical imaging, NIR light and SWIR light correspond to the first 'biological window' (~650–950 nm) and the second 'biological window' (~1000–1400 nm)[6,7], respectively, producing low optical scattering and absorption in tissues (especially for SWIR light) and thus enabling deep-tissue imaging[8–10]. More importantly, the 'self-illuminating' feature of persistent luminescence allows the imaging to be conducted in an excitation-free and, hence, autofluorescence-free manner, enabling a high signal-to-noise ratio and exceptional imaging sensitivity[11]. As a result of extensive research, an array of Cr^{3+}-activated gallate-based NIR persistent phosphors (for example, $Zn_3Ga_2Ge_2O_{10}$:Cr^{3+} and $LiGa_5O_8$:Cr^{3+})[12–16], emitting at 690–750 nm with a very-long afterglow of >100 h, were recently discovered and synthesized and quickly found exciting applications in biomedical imaging[17,18]. In contrast, however, reliable persistent phosphors emitting in the SWIR spectral region are lacking. A few phosphors were found to emit short-duration SWIR afterglow but were accompanied by dominant visible persistent luminescence from the dopants or the host compositions[19,20].

Trivalent ytterbium (Yb^{3+}) has only two manifolds in the 4f shell, that is, a $^2F_{7/2}$ ground state and a $^2F_{5/2}$ excited state, with an energy difference between the states of ~10 000 cm^{-1}. Typical emission for Yb^{3+}-activated phosphors features a fine-structure spectral shape owing to the Stark splitting of the two Yb^{3+} manifolds, as shown schematically in the inset of Figure 1a. This simple and unique energy-level structure endows Yb^{3+} with several fascinating optical properties, including no absorption in the visible range, strong absorption near 980 nm (well-suited for InGaAs diode laser emission), and intense emission at 950–1150 nm ($^2F_{5/2} \rightarrow {}^2F_{7/2}$ transition; in the SWIR range)[21]. Accordingly, the Yb^{3+} ion has been extensively studied over the past two decades for use in a variety of important applications, for instance, as the emitter in InGaAs diode-pumped solid-state SWIR lasers[22,23], as the sensitizer (by absorbing 980 nm photons) to activate other

[1]College of Engineering, University of Georgia, Athens, GA 30602, USA; [2]Key Laboratory for Liquid-Solid Structure Evolution and Processing of Materials, Shandong University, Jinan 250061, China; [3]Department of Physics and Astronomy, University of Georgia, Athens, GA 30602, USA and [4]Department of Physics, Georgia Southern University, Statesboro, GA 30460, USA
*These authors contributed equally to this work.
Correspondence: ZW Pan, Email: panz@uga.edu; KN Sun, Email: sunkangning@sdu.edu.cn
Received 3 November 2015; revised 29 February 2016; accepted 2 March 2016; accepted article preview online 3 March 2016

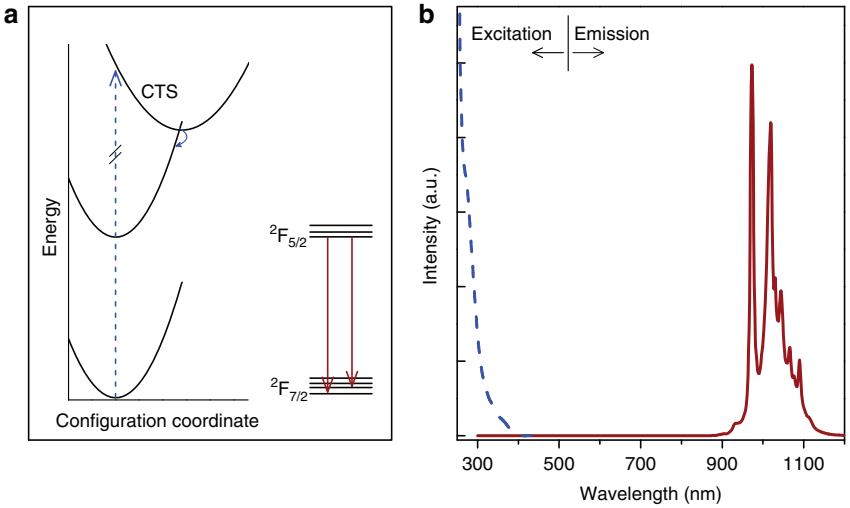

Figure 1 Energy diagram of the Yb^{3+} ion and photoluminescence spectra of the $MgGeO_3$:Yb^{3+} phosphor. (**a**) Configuration coordinate diagram of the Yb^{3+} charge transfer state (CTS) and Yb^{3+} 4*f* ground ($^2F_{7/2}$) and excited ($^2F_{5/2}$) states. The inset is the Stark energy level diagram of Yb^{3+}. (**b**) Normalized photoluminescence excitation and emission spectra of $MgGeO_3$:Yb^{3+} phosphor at room temperature. The emission spectrum is acquired under 300-nm light excitation, and the excitation spectrum is obtained by monitoring the 1019-nm emission.

lanthanide ions (for example, Er^{3+} ion) for up-conversion luminescence[24,25], and as the spectral converter in Ln^{3+}-Yb^{3+} doubly doped quantum cutting phosphors for high-efficiency Si photovoltaics (the emission of Yb^{3+} at ~1000 nm perfectly matches the maximum spectral response of Si solar cells)[26,27]. In addition to the unique energy-level structure, Yb^{3+} also has a unique $4f^{13}$ electronic configuration, which can easily gain one electron to reach the more stabilized $4f^{14}$ configuration of the full shell. This tendency of reduction to Yb^{2+} enables the Yb^{3+} ion in some hosts, such as oxides[28], fluorides[28], oxysulfides[29] and nitrides[30], to receive an electron from the host's anion under high-energy external excitation (for example, ultraviolet (UV) light), forming a charge transfer state (CTS). The CTS of Yb^{3+} can transfer the excitation energy to the $^2F_{5/2}$ emitting state via a non-radiative relaxation process (Figure 1a), giving SWIR photoluminescence at around 1000 nm.

Here we report on a new function of the Yb^{3+} ion—as an emitter for SWIR persistent luminescence. We have developed the first real SWIR persistent phosphor, Yb^{3+}-doped $MgGeO_3$, which exhibits a very long SWIR persistent luminescence at around 1000 nm for more than 100 h after UV light excitation. The $MgGeO_3$:Yb^{3+} phosphor is a promising UV-to-SWIR spectral convertor as well as a superb storage phosphor, exhibiting a photostimulated persistent luminescence capability.

MATERIALS AND METHODS

Materials synthesis

The $MgGeO_3$:Yb^{3+} phosphor was fabricated using a high-temperature solid-state reaction technique. Stoichiometric amounts of MgO and GeO_2 powders and 0.05 mol% Yb_2O_3 powder (the corresponding Yb^{3+} concentration is 0.1 mol%) were thoroughly mixed and ground in an agate mortar. The mixed powder was pressed into preformed discs (~15 mm in diameter and ~1 mm in thickness) using a 16-T dry pressing machine. The discs were then sintered at 1250 °C in air for 2 h to form solid ceramic discs.

Characterization methods

The crystal structure of the as-synthesized $MgGeO_3$:Yb^{3+} phosphor was characterized on a PANalytical X'Pert PRO powder X-ray diffractometer (PANalytical Inc., Westborough, MA, USA) with Cu $K\alpha_1$ radiation ($\lambda = 1.5406$ Å). The spectral properties, including the photoluminescence emission and excitation spectra, persistent luminescence decay curves, persistent luminescence excitation spectra and photostimulated persistent luminescence (PSPL) properties, of the phosphor were analyzed using a Horiba FluoroLog-3 spectrofluorometer (Horiba Scientific, Edison, NJ, USA) equipped with a 450-W xenon arc lamp, a photomultiplier tube (measurement range, 240–850 nm) and a InGaAs detector (measurement range, 800–1600 nm). The thermoluminescence spectra were recorded using a homemade thermoluminescence setup (temperature range, 20–280 °C; heating rate, 4 °C per second). Before all the spectral measurements, the samples were heat-treated in a furnace at 450 °C to completely empty the energy traps in the material. A 4-W, 254-nm UV lamp was also used to excite the samples. A white light emitting diode (LED) flashlight (with an output of ~1 mW cm^{-2}) and a 100-mW 808-nm NIR laser were used as the illumination sources in the PSPL measurements.

RESULTS AND DISCUSSION

X-ray diffraction measurements show that the as-synthesized $MgGeO_3$:0.1 mol% Yb^{3+} phosphor is ilmenite structured $MgGeO_3$ (Supplementary Fig. S1). Although the ionic radius of the Yb^{3+} ion (0.087 nm for six coordination) is larger than that of the Mg^{2+} ion (0.072 nm for six coordination), the Yb^{3+} ion most probably occupies the Mg^{2+} site in the $MgGeO_3$ lattice. The substitution of Mg^{2+} with Yb^{3+} distorts the lattice and requires secondary impurities to offer local charge compensation. Therefore, the Yb^{3+} concentration in $MgGeO_3$ is limited to be very low (<0.5 mol%) (Supplementary Fig. S1).

Figure 1b shows the normalized photoluminescence emission and excitation spectra of $MgGeO_3$:Yb^{3+} phosphor at room temperature. Under the excitation of 300 nm light, the material exhibits an intense photoluminescence at 930–1150 nm, featuring a fine spectral structure with two main peaks at 980 and 1019 nm and several weak peaks at 1020–1100 nm, which correspond to different optical transitions between the Stark levels of the $^2F_{5/2}$ and $^2F_{7/2}$ states. The excitation spectrum (monitoring 1019 nm emission) covers only the UV spectral

doi:10.1038/lsa.2016.124

region from 250 to 400 nm (250 nm is the measurement limit of our spectrofluorometer). The high-energy side (<260 nm) of the excitation spectrum may be assigned to the fundamental absorption edge of the host, while the excitation shoulder on the low-energy side (300–400 nm) is attributed to the absorption of CTS[28], which can efficiently transfer excitation energy to the $^2F_{5/2}$ emitting states, followed by the $^2F_{5/2} \rightarrow {}^2F_{7/2}$ transition. Figure 1b also shows that there is no excitation or emission from either the Yb^{3+} emitter or the $MgGeO_3$ host in the visible–NIR spectral region (~400–900 nm), indicating that the $MgGeO_3$:Yb^{3+} phosphor is spectrally transparent to the visible and NIR light and that the $MgGeO_3$:Yb^{3+} phosphor is a promising UV-to-SWIR spectral convertor.

When the UV excitation ceased, very long-lasting persistent luminescence in the 930–1150 nm range was observed in the $MgGeO_3$:Yb^{3+} phosphor. Figure 2a shows the persistent luminescence decay curve of the $MgGeO_3$:Yb^{3+} phosphor monitoring at 1019 nm after the sample was irradiated with a 254-nm UV lamp for 15 min. The intensity of the persistent emission decreases quickly in the first half an hour and then slowly over time. After 6 h of decay, the intensity of the persistent emission is still considerably high. The inset of Figure 2a shows a persistent luminescence emission spectrum acquired at 30 min after the removal of the excitation. The persistent luminescence emission spectrum shares an identical profile with the photoluminescence emission spectrum (Figure 1b), indicating that the SWIR persistent luminescence originates from the Yb^{3+} emitting centers. Remarkably, the Yb^{3+} persistent luminescence can be recorded even after 100 h of decay (Supplementary Fig. S2), showing that the SWIR persistence time of the $MgGeO_3$:Yb^{3+} phosphor is longer than 100 h. We also studied the effects of excitation duration on the charging capability and the persistent luminescence performance of the phosphor. Within 15 min of excitation using a 254-nm UV lamp, there is a direct relationship between the persistent luminescence intensity and the excitation duration; over 15 min of excitation, the material appears to be fully charged (Supplementary Fig. S3).

We also determined the effectiveness of different excitation energies in producing SWIR persistent luminescence in $MgGeO_3$:Yb^{3+} by studying the relationship between the intensity of persistent luminescence and the excitation wavelength. In our experiments, we excited the material using different wavelengths between 260 and 450 nm in 5 nm steps, and acquired the persistent luminescence decay curve (monitoring at 1019 nm emission) after each excitation (Supplementary Fig. S4). The intensity of the persistent emission at a decay time of 30 s (I_{30s}; indicated by the vertical line in Supplementary Fig. S4) was used as the reference point to plot the persistent luminescence excitation spectrum, as shown in Figure 2b. For comparison, the photoluminescence excitation spectrum in Figure 1b is re-displayed in Figure 2b. The excitation spectrum for persistent luminescence is different from that for photoluminescence. The SWIR persistent luminescence in $MgGeO_3$:Yb^{3+} can only be achieved by UV irradiation with wavelengths shorter than ~320 nm (see inset of Figure 2b; showing that the onset wavelength for achieving persistent luminescence is at ~320 nm) and the effectiveness increases sharply as the excitation moves to shorter wavelengths. The irradiation with wavelengths between 320 and 400 nm, which can effectively produce SWIR photoluminescence via the excitation of the CTS of Yb^{3+} (Figure 1a), does not produce persistent luminescence in $MgGeO_3$:Yb^{3+} because the Yb^{3+} persistent luminescence in $MgGeO_3$ has a different excitation mechanism from Yb^{3+} photoluminescence.

Under ambient conditions, we observed that UV irradiation can cause the body color of $MgGeO_3$:Yb^{3+} discs to change from white to beige, as the digital picture shown in Figure 3. This coloration phenomenon is long-lived, taking several days for the discs to restore their original white body color, and the coloration can repeatedly occur upon UV irradiation. The occurrence of coloration in $MgGeO_3$:Yb^{3+} can be ascribed to the creation of a photochromic center[31,32], which may arise from the trapping of photogenerated electrons by lattice defects, for example, oxygen vacancies, in the host (note: oxygen vacancies were identified as effective electron trapping centers in the $MgGeO_3$ host[33]. Moreover, undoped $MgGeO_3$ also exhibits weak coloration phenomenon). Our previous study on $LiGa_5O_8$:Cr^{3+} NIR persistent phosphor[13], which also exhibits similar coloration phenomenon, has revealed that the photochromic centers in persistent phosphors may serve as deep energy traps for photogenerated

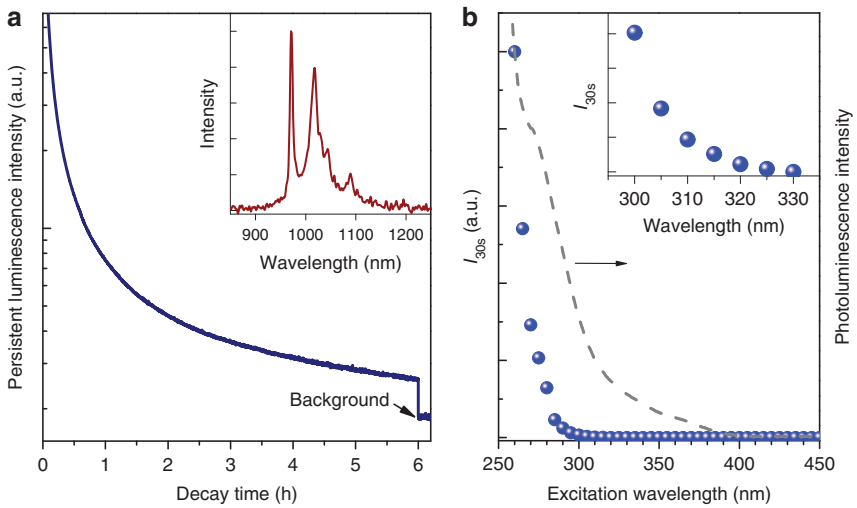

Figure 2 Persistent luminescence properties of $MgGeO_3$:Yb^{3+} phosphor at room temperature. (**a**) Persistent luminescence decay curve monitored at 1019 nm after irradiation by a 254-nm UV lamp for 15 min. The inset shows the persistent luminescence emission spectrum recorded at 30 min after stopping the irradiation. (**b**) Persistent luminescence excitation spectrum obtained by plotting the persistent luminescence intensity (I_{30s}) monitored at 1019 nm as a function of the excitation wavelengths over the 260–450 nm spectral range. The sample was irradiated for 5 min at each measured wavelength using a xenon arc lamp. The dash-line curve shows the photoluminescence excitation spectrum monitored at 1019 nm.

Figure 3 UV-irradiation-induced coloration of the $MgGeO_3$:Yb^{3+} phosphor. Digital picture of an $MgGeO_3$:Yb^{3+} phosphor disc. The right side of the disc was irradiated by a 254-nm UV lamp for 5 min, while the left side was covered by a piece of paper. UV irradiation causes the body color to change from white to beige.

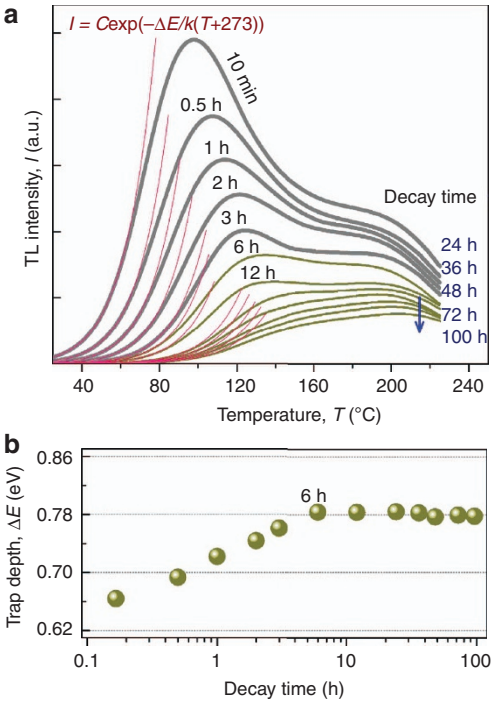

Figure 4 Thermoluminescence curves and trap depths of the $MgGeO_3$:Yb^{3+} phosphor. (**a**) Thermoluminescence curves monitored at 1019 nm emission over 20–230 °C for samples undergoing different decay times from 10 min to 100 h. The samples were pre-irradiated by a 254-nm UV lamp for 15 min. The red curves at the low temperature side are fit using an initial rise analysis method (see text for further details). (**b**) Plot of the trap depths as a function of decay times. The trap depths were obtained from the fittings in **a**.

electrons. To understand the nature of photochromic centers and the distribution of energy traps in $MgGeO_3$:Yb^{3+}, we conducted thermoluminescence measurements at 25–230 °C by monitoring the 1019-nm emission on $MgGeO_3$:Yb^{3+} samples undergoing different decay times from 10 min to 100 h after excitation, as the thermoluminescence curves displayed in Figure 4a. For the case of 10 min short decay, the thermoluminescence curve exhibits two broad bands with band maxima at ~100 °C (low-temperature band) and ~200 °C (high-temperature band). With the increase of decay time, the intensity of the low-temperature band decreases sharply, and the lower-temperature side of the band decreases, resulting in the band maximum moving to higher temperature. After 12 h of decay, most of the low-temperature band disappears. For the high-temperature band, however, while its intensity gradually decreases with decay time, the position of the band maximum almost remains unchanged. After 100 h of decay, the high-temperature band is still significant, meaning that a considerable amount of trapped electrons were still not released after 100 h of natural decay. The thermoluminescence results are therefore consistent with the persistent luminescence emission measurements shown in Supplementary Fig. S2.

Because the spectral shape of a thermoluminescence curve is correlated to trap distribution[34], the change of the thermoluminescence curve profiles with decay time in Figure 4a shows the emptying process of traps in material during the persistent luminescence process, that is, the shallow traps are emptied first, followed by the emptying of the deep traps. Based on the thermoluminescence curves in Figure 4a, we determined the trap depths corresponding to different decay times in $MgGeO_3$:Yb^{3+} using an initial rise analysis method[35], in which the shallowest trap occupied at each decay time was evaluated by fitting the low-temperature sides of the thermoluminescence curves using $I(T) = C\exp(-\Delta E/k(T+273))$, where I is the thermoluminescence intensity, T is the temperature, ΔE is the trap depth, C is a fitting constant and k is the Boltzmann constant. The fittings are shown as the red curves in Figure 4a (the fittings are also drawn in $\ln(I)$ versus $1/T$ coordinates, as shown in Supplementary Fig. S5). The obtained trap depths (ΔE) are plotted as a function of decay times, as the ball curve shown in Figure 4b. As the decay time increases from 10 min to 6 h, the trap depth increases from ~0.66 to ~0.78 eV. The gradual deepening of the trap depth along with the decay time indicates the presence of a continuous trap distribution in $MgGeO_3$:Yb^{3+} (ref. 35). When the decay time is over 6 h, the trap depth remains almost unchanged at ~0.78 eV. This constant trap depth is a strong indicator of the presence of deep traps corresponding to the photochromic centers[13], whose ground state is located at ~0.78 eV below the conduction band of $MgGeO_3$. Therefore, there are two types of traps in $MgGeO_3$:Yb^{3+}, that is, the shallow traps with continuous trap distribution and the high-energy photochromic-center-type deep traps.

To further understand the photochromic centers and their role in persistent luminescence, we conducted thermoluminescence measurements after photostimulation on 120-h-decayed $MgGeO_3$:Yb^{3+} samples, as shown in Figure 5a. The photostimulation technique has been routinely used to investigate the photochromic centers in storage phosphors[36] and was recently used by us to study the photochromism in $LiGa_5O_8$:Cr^{3+} NIR persistent phosphor[13]. The solid-line curve and dash-line curve in Figure 5a show the thermoluminescence spectra of a 120-h-decayed $MgGeO_3$:Yb^{3+} sample with and without white LED flashlight illumination (for 120 s), respectively (the emission spectrum

doi:10.1038/lsa.2016.124

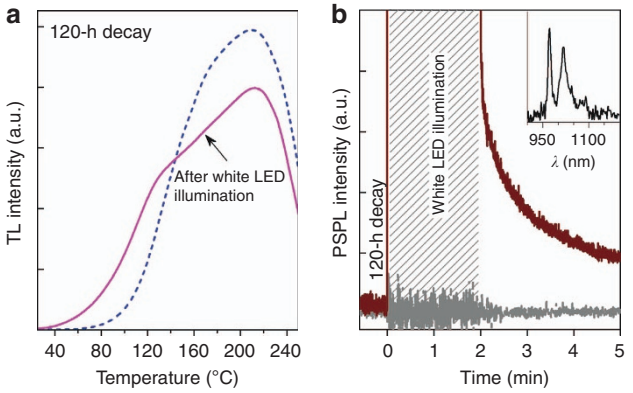

Figure 5 Photostimulation of the $MgGeO_3$:Yb^{3+} phosphor. (**a**) Thermoluminescence curves monitored at 1019-nm emission over 20–250 °C on 120-h-decayed samples with (solid-line curve) and without (dash-line curve) white LED stimulation. The samples were pre-irradiated by a 254-nm UV lamp for 15 min. The white LED stimulation time was 120 s. (**b**) PSPL decay curves monitored at 1019 nm. The brown curve was acquired on a 120-h-decayed sample (pre-irradiated by a 254-nm UV lamp for 15 min), while the gray curve was recorded on a fresh sample (without UV pre-irradiation). The inset is the PSPL emission spectrum of the 120-h-decayed sample, which was recorded at 1 min after stopping the stimulation.

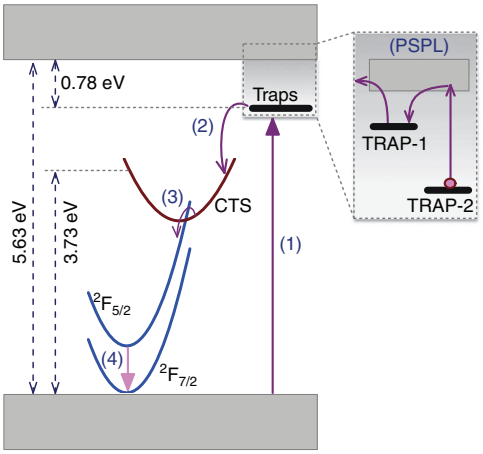

Figure 6 A schematic representation of SWIR persistent luminescence and SWIR PSPL mechanisms in $MgGeO_3$:Yb^{3+}. The band energy of the $MgGeO_3$ host, the energy level of the CTS of Yb^{3+} and the depth of the deep traps are drawn to scale. The straight-line arrows and curved-line arrows represent optical transitions and electron transfer processes (see text for further details), respectively.

of the flashlight is shown in Supplementary Fig. S6). The white LED illumination significantly modifies the thermoluminescence spectrum profile: the intensity of the high-temperature band decreases, and part of the low-temperature band reappears. Because low-energy white light cannot directly fill the energy traps (including the shallow traps) in $MgGeO_3$:Yb^{3+} (Figure 2b), the changes in the thermoluminescence curve profiles indicate that the white LED illumination causes the remaining trapped electrons (due to UV pre-irradiation) in the material to redistribute: some electrons in the deep traps are photoliberated, while some shallow traps are refilled.

The photostimulation-induced refilling of the shallow traps is expected to enhance the persistent luminescence intensity of the decayed $MgGeO_3$:Yb^{3+} phosphor at room temperature[13]. When a 120-h-decayed $MgGeO_3$:Yb^{3+} disc was illuminated with a white LED flashlight for 120 s, the persistent luminescence was rejuvenated and the persistent luminescence intensity was significantly enhanced, as the persistent luminescence decay curve (brown curve) shown in Figure 5b (note that this phenomenon also occurs with red light (>590 nm) or NIR light (for example, 808 nm) illumination, as shown in Supplementary Fig. S7). This low-energy light illumination-induced persistent luminescence has been called PSPL[13]. The inset of Figure 5b shows the PSPL emission spectrum of the 120-h-decayed $MgGeO_3$:Yb^{3+} sample recorded at 1 min after stopping the stimulation. The PSPL emission spectrum has an identical profile to the photoluminescence emission spectrum (Figure 1b) and the persistent luminescence emission spectrum (inset of Figure 2b). In PSPL, the essential excitation source is UV pre-irradiation. The low-energy white light (or red light or NIR light) illumination just triggers the liberation of the trapped electrons in deep traps, leading to subsequent electron transfer to shallow traps for enhanced and prolonged persistent luminescence. To show the critical role of UV pre-irradiation in the generation of the enhanced SWIR PSPL signal, we also performed the photostimulation experiment on a fresh $MgGeO_3$:Yb^{3+} sample (that is, without UV pre-irradiation), as shown in the gray curve in Figure 5b. As expected, no persistent luminescence signal was detected in the fresh sample. The PSPL phenomenon observed in $MgGeO_3$:Yb^{3+} phosphor has promising implications for biomedical imaging. For example, the PSPL capability enables the $MgGeO_3$:Yb^{3+} phosphor (in the form of nanoparticles) pre-irradiated by UV light *in vitro* to be activated *in vivo* by high-tissue-penetrating low-energy light, giving rise to an enhanced SWIR PSPL signal that can greatly expand the imaging duration[17].

On the basis of the above results, we propose a model to interpret the SWIR persistent luminescence and the SWIR PSPL mechanisms in $MgGeO_3$:Yb^{3+}, as schematically shown in Figure 6. In Figure 6, the band energy of the $MgGeO_3$ host[37], the energy level of the CTS of Yb^{3+} and the depth of the deep traps obtained in this study are drawn to scale. To simplify the discussion, we assign the shallow traps with continuous trap distribution and the filled deep traps (that is, the photochromic centers) as TRAP-1 and TRAP-2, respectively. Under high-energy UV excitation (for example, 254 nm), the traps (TRAP-1 and TRAP-2) are directly filled via electron excitation from the top of the valence band (process 1). This excitation transition is allowed in principle because the traps are oxygen-vacancy type[33], whose electronic composition is generally identical to that of the conduction-band bottom (the oxygen-vacancy type traps are further testified in the Pr^{3+}-activated $MgGeO_3$ SWIR persistent phosphor, as shown in the results in Supplementary Fig. S8). In the persistent luminescence process, the trapped electrons recombine with the CTS (process 2). The excited state of Yb^{3+} is subsequently populated via an intersystem crossing process (process 3), followed by the persistent luminescence emission from $^2F_{5/2}$ to $^2F_{7/2}$ (process 4). For the PSPL process (right panel in Figure 6), after an initial decay at room temperature, TRAP-1 is thermally emptied. With the stimulation of low-energy light (for example, white light), some trapped electrons in TRAP-2 are liberated and promoted to the conduction band, resulting in the refilling of the depleted TRAP-1. As a result, the persistent luminescence signal is enhanced, that is, PSPL in the SWIR occurs.

Finally, besides the $MgGeO_3$:Yb^{3+} phosphor, SWIR persistent luminescence was also obtained in Yb^{3+}-doped gallate-based host materials, such as $LiGa_5O_8$, $Zn_3Ga_2GeO_8$ and $La_3Ga_5GeO_{14}$, as shown in Supplementary Fig. S9 (these gallates are also excellent hosts for Cr^{3+} NIR persistent luminescence[12–15]).

CONCLUSIONS

We found a new function for the Yb^{3+} ion—as an emitter for SWIR persistent luminescence—and developed the first real SWIR persistent phosphor, $MgGeO_3$:Yb^{3+}. The $MgGeO_3$:Yb^{3+} phosphor exhibits SWIR persistent luminescence at around 1000 nm, with a long persistence time of more than 100 h. UV-light pre-irradiated $MgGeO_3$:Yb^{3+} samples also exhibit a photostimulated persistent luminescence capability after short stimulation by low-energy white or red light. The Yb^{3+}-activated SWIR persistent phosphors are expected to have applications in biomedical imaging, night-vision surveillance and Si photovoltaics.

CONFLICT OF INTEREST

The authors declare no conflict of interest.

ACKNOWLEDGEMENTS

ZWP acknowledges financial support from the National Science Foundation (CAREER DMR-0955908, DMR-1403929). KNS is grateful for the financial support from the National Natural Science Foundation of China (no. 81171463). YJL and YFC acknowledge support from the China Scholarship Council. FL is grateful for the helpful discussion with Pieter Dorenbos.

1 Hölsä J. Persistent luminescence beats the afterglow: 400 years of persistent luminescence. *Electrochem Soc Interface* 2009; **18**: 42–45.
2 Yen WM, Shionoya S, Yamamoto H. *Phosphor Handbook*. Boca Raton: CRC Press; 2007.
3 Matsuzawa T, Aoki Y, Takeuchi N, Murayama Y. A new long phosphorescent phosphor with high brightness, $SrAl_2O_4$: Eu^{2+}, Dy^{3+}. *J Electrochem Soc* 1996; **143**: 2670–2673.
4 Lin YH, Tang ZL, Zhang ZT, Wang XJ, Zhang JY. Preparation of a new long afterglow blue-emitting $Sr_2MgSi_2O_7$-based photoluminescent phosphor. *J Mater Sci Lett* 2001; **20**: 1505–1506.
5 Driggers RG, Hodgkin V, Vollmerhausen R. What good is SWIR? Passive day comparison of VIS, NIR, and SWIR. *Proc SPIE*, 2013; **8706**: 87060L.
6 Smith AM, Mancini MC, Nie SM. Bioimaging: second window for *in vivo* imaging. *Nat Nanotechnol* 2009; **4**: 710–711.
7 Friebel M, Helfmann J, Netz U, Meinke M. Influence of oxygen saturation on the optical scattering properties of human red blood cells in the spectral range 250 to 2000 nm. *J Biomed Opt* 2009; **14**: 034001.
8 Naczynshi DJ, Tan MC, Zevon M, Wall B, Kohl J *et al.* Rare-earth-doped biological composites as *in vivo* shortwave infrared reporters. *Nat Commun* 2013; **4**: 2199.
9 Lim YT, Kim S, Nakayama A, Stott NE, Bawendi MG *et al.* Selection of quantum dot wavelengths for biomedical assays and imaging. *Mol Imaging* 2003; **2**: 50–64.
10 Welsher W, Liu Z, Sherlock SP, Robinson JT, Chen Z *et al.* A route to brightly fluorescent carbon nanotubes for near-infrared imaging in mice. *Nat Nanotechnol* 2009; **4**: 773–780.
11 de Chermont QLM, Chanéac C, Seguin J, Pellé F, Maîtrejean S *et al.* Nanoprobes with near-infrared persistent luminescence for *in vivo* imaging. *Proc Natl Acad Sci USA* 2007; **104**: 9266–9271.
12 Pan ZW, Lu YY, Liu F. Sunlight-activated long-persistent luminescence in the near-infrared from Cr^{3+}-doped zinc gallogermanates. *Nat Mater* 2012; **11**: 58–63.
13 Liu F, Yan WZ, Chuang YJ, Zhen ZP, Xie J *et al.* Photostimulated near-infrared persistent luminescence as a new optical read-out from Cr^{3+}-doped $LiGa_5O_8$. *Sci Rep* 2013; **3**: 1554.
14 Yan WZ, Liu F, Lu YY, Wang XJ, Yin M *et al.* Near infrared long-persistent phosphorescence in $La_3Ga_5GeO_{14}$: Cr^{3+} phosphor. *Opt Express* 2010; **18**: 20215–20221.
15 Jia D, Lewis LA, Wang XJ. Cr^{3+}-doped lanthanum gallogermanate phosphors with long persistent IR emission. *Electrochem Solid-State Lett* 2010; **13**: J32–J34.
16 Bessière A, Jacquart S, Priolkar K, Lecointre A, Viana B *et al.* $ZnGa_2O_4$: Cr^{3+}: a new red long-lasting phosphor with high brightness. *Opt Express* 2011; **19**: 10131–10137.
17 Chuang YJ, Zhen ZP, Zhang F, Liu F, Mishra JP *et al.* Photostimulable near-infrared persistent luminescent nanoprobes for ultrasensitive and longitudinal deep-tissue bio-imaging. *Theranostics* 2014; **4**: 1112–1122.
18 Abdukayum A, Chen JT, Zhao Q, Yan XP. Functional near infrared-emitting Cr^{3+}/Pr^{3+} Co-doped zinc gallogermanate persistent luminescent nanoparticles with super-long afterglow for *in vivo* targeted bioimaging. *J Am Chem Soc* 2013; **135**: 14125–14133.
19 Yu NY, Liu F, Li XF, Pan ZW. Near infrared long-persistent phosphorescence in $SrAl_2O_4$: Eu^{2+}, Dy^{3+}, Er^{3+} phosphors based on persistent energy transfer. *Appl Phys Lett* 2009; **95**: 231110.
20 Kamimura S, Xu CN, Yamada H, Terasaki N, Fujihala M. Long-persistent luminescence in the near-infrared from Nd^{3+}-doped Sr_2SnO_4 for *in vivo* optical imaging. *Jpn J Appl Phys* 2014; **53**: 092403.
21 Boulon G. Why so deep research on Yb^{3+}-doped optical inorganic materials? *J Alloy Compd* 2008; **451**: 1–11.
22 Brenier A, Boulon G. Overview of the best Yb^{3+} doped laser crystals. *J Alloy Compd* 2001; **323-324**: 210–213.
23 Cascales C, Serrano MD, Esteban-Betegón F, Zaldo C. Structural, spectroscopic, and tunable laser properties of Yb^{3+}-doped $NaGd(WO_4)_2$. *Phys Rev B* 2006; **74**: 174114.
24 Heer S, Kömpe K, Güdel HU, Haase M. Highly efficient multicolour upconversion emission in transparent colloids of lanthanide-doped $NaYF_4$ nanocrystals. *Adv Mater* 2004; **16**: 2102–2105.
25 Wang F, Liu XG. Upconversion multicolor fine-turning: visible to near-infrared emission from lanthanide-doped $NaYF_4$ nanoparticles. *J Am Chem Soc* 2008; **130**: 5642–5643.
26 van der Ende BM, Aarts L, Meijerink A. Near-infrared quantum cutting for photovoltaics. *Adv Mater* 2009; **21**: 3073–3077.
27 Zhang QY, Huang XY. Recent progress in quantum cutting phosphors. *Prog Mater Sci* 2010; **55**: 353–427.
28 van Pieterson L, Heeroma M, de Heer E, Meijerink A. Charge transfer luminescence of Yb^{3+}. *J Lumin* 2000; **91**: 177–193.
29 Zhang GG, Liu CM, Wang J, Kuang XJ, Su Q. An intense charge transfer broadband sensitized near-infrared emitting $CaLaGa_3S_6O$: Yb^{3+} phosphor suitable for solar spectral convertor. *Opt Express* 2011; **19**: 24314–24319.
30 ten Kate OM, Hintzen HT, Dorenbos P, van der Kolk E. Yb^{3+} doped $LaSi_3N_5$ and YSi_3N_5 with low energy charge transfer for near-infrared light-emitting diode and solar cell application. *J Mater Chem* 2011; **21**: 18289–18294.
31 Hosono H, Asada N, Abe Y. Properties and mechanism of photochromism in reduced calcium aluminate glass. *J Appl Phys* 1990; **67**: 2840–2847.
32 Qiu JB, Makishima A. Ultraviolet-radiation-induced structure and long-lasting phosphorescence in Sn^{2+}-Cu^{2+} co-doped silicate glass. *Sci Technol Adv Mater* 2003; **4**: 35–38.
33 Iwasaki M, Kim DN, Tanaka K, Murata T, Morinaga K. Red phosphorescence properties of Mn ions in MgO-GeO_2 compounds. *Sci Technol Adv Mater* 2003; **4**: 137–142.
34 Dorenbos P, Bos AJJ. Lanthanide level location and related thermoluminescence phenomena. *Radiat Meas* 2008; **43**: 139–145.
35 van den Eeckhout K, Bos AJJ, Poelman D, Smet PF. Revealing trap depth distribution in persistent phosphors. *Phys Rev B* 2013; **87**: 045126.
36 Schweizer S. Physics and current understanding of X-ray storage phosphors. *Physica Status Solidi A Appl Res* 2001; **187**: 335–393.
37 Katayama Y, Ueda J, Tanabe S. Effect of Bi_2O_3 doping on persistent luminescence of $MgGeO_3$: Mn^{2+} phosphor. *Opt Mater Express* 2014; **4**: 613–623.

Supplementary Information for this article can be found on the *Light: Science & Applications*' website (http://www.nature.com/lsa).